Structure-based Design of Novel Small-Molecule Inhibitors of *Plasmodium falciparum*

Sandhya Kortagere,*,† William J. Welsh,‡ Joanne M. Morrisey,† Thomas Daly,† Ijeoma Ejigiri,§ Photini Sinnis,§ Akhil B. Vaidya,† and Lawrence W. Bergman†

Center for Molecular Parasitology, Department of Microbiology and Immunology, Drexel University College of Medicine, 2900 Queen Lane, Philadelphia, Pennsylvania, Department of Pharmacology, University of Medicine and Dentistry of New Jersey, Robert Wood Johnson Medical School, 675 Hoes Lane, Piscataway, New Jersey, and Department of Molecular Parasitology, New York University School of Medicine, 550 1st Avenue, New York, New York

Received January 27, 2010

Malaria is endemic in most developing countries, with nearly 500 million cases estimated to occur each year. The need to design a new generation of antimalarial drugs that can combat the most drug-resistant forms of the malarial parasite is well recognized. In this study, we wanted to develop inhibitors of key proteins that form the invasion machinery of the malarial parasite. A critical feature of host-cell invasion by apicomplexan parasites is the interaction between the carboxy terminal tail of myosin A (MyoA) and the myosin tail interacting protein (MTIP). Using the cocrystal structure of the *Plasmodium knowlesi* MTIP and the MyoA tail peptide as input to the hybrid structure-based virtual screening approach, we identified a series of small molecules as having the potential to inhibit MTIP−MyoA interactions. Of the initial 15 compounds tested, a pyrazole−urea compound inhibited *P. falciparum* growth with an EC_{50} value of 145 nM. We screened an additional 51 compounds belonging to the same chemical class and identified 8 compounds with EC_{50} values less than 400 nM. Interestingly, the compounds appeared to act at several stages of the parasite's life cycle to block growth and development. The pyrazole−urea compounds identified in this study could be effective antimalarial agents because they competitively inhibit a key protein−protein interaction between MTIP and MyoA responsible for the gliding motility and the invasive features of the malarial parasite.

INTRODUCTION

Each year, an estimated 500 million cases of malaria occur worldwide, resulting in as many as three million deaths, mostly in young children and pregnant women.[1] Approximately 40% of the world's population is at risk of contracting malaria; the scale of human suffering and the economic loss caused by this disease are staggering.[2] Although several drugs are available for treating malaria, the widespread resistance to the most affordable drugs and the emerging resistance to alternative drugs as well as their high cost are major impediments in efforts to control this disease. Clearly, new affordable antimalarial agents with reduced propensity to develop resistance are urgently needed. Among the four malarial parasites that infect the human host, *Plasmodium falciparum* is the most lethal form and is responsible for 95% of the three million deaths resulting from this disease.[1] Recent reports of potential artemisinin-resistant parasites in East Asia have spurred various national and international agencies to stop the spread of these parasites.[3] Apart from the issue of acquired drug resistance by the parasite, another major challenge facing those engaged in drug development is the toxic side effects of the drugs themselves.[4] Targeting novel pathways that are exclusive to the parasite offer a fruitful strategy for discovering drugs that demonstrates an acceptable selectivity for the parasite over the human host and, hence, that carries less risk of adverse reactions. Examples of small-molecule antimalarial compounds include inhibitors of the de novo synthesis pathway of pyrimidine nucleotides in *P. vivax* and *P. falciparum*, which allows the alternative salvage pathway in humans[5] and inhibitors of dihydroorotate dehydrogenase that catalyzes the oxidation of the intermediate dihydroorotate to orotate[6] and orotidine 5′-monophosphate decarboxylase.[7] Also, 20S proteasome,[8] cytochrome bc_1 complex,[9] and other enzymes, such as arginine methyltransferases,[10] carbonic anhydrases,[11] protein-dependent kinase-1,5,[12] and cysteine proteases[13] have been successfully targeted with small molecules and peptides in an effort to derive novel antimalarial compounds. At present, however, only a limited number of chemical scaffolds and targets are in clinical use for treating malaria. As resistance to these entities emerges, it is important to have new scaffolds in the pipeline to circumvent cross-resistance. The urgent need to target the drug-resistant forms of the *P. falciparum* parasite has stimulated new directions in antimalarial drug development. Several groups are investigating different drug dosing regimens or drug combinations as a strategy to treat malaria.[14] Another strategy for overcoming microbial drug resistance is to devise new molecular scaffolds that are unrelated to current drugs that can inhibit key protein−protein interactions. One such protein−protein interaction that is key

* Corresponding author. E-mail: sandhya.kortagere@drexelmed.edu.
† Drexel University College of Medicine.
‡ University of Medicine and Dentistry of New Jersey.
§ New York University School of Medicine.

10.1021/ci100039k © 2010 American Chemical Society
Published on Web 04/28/2010

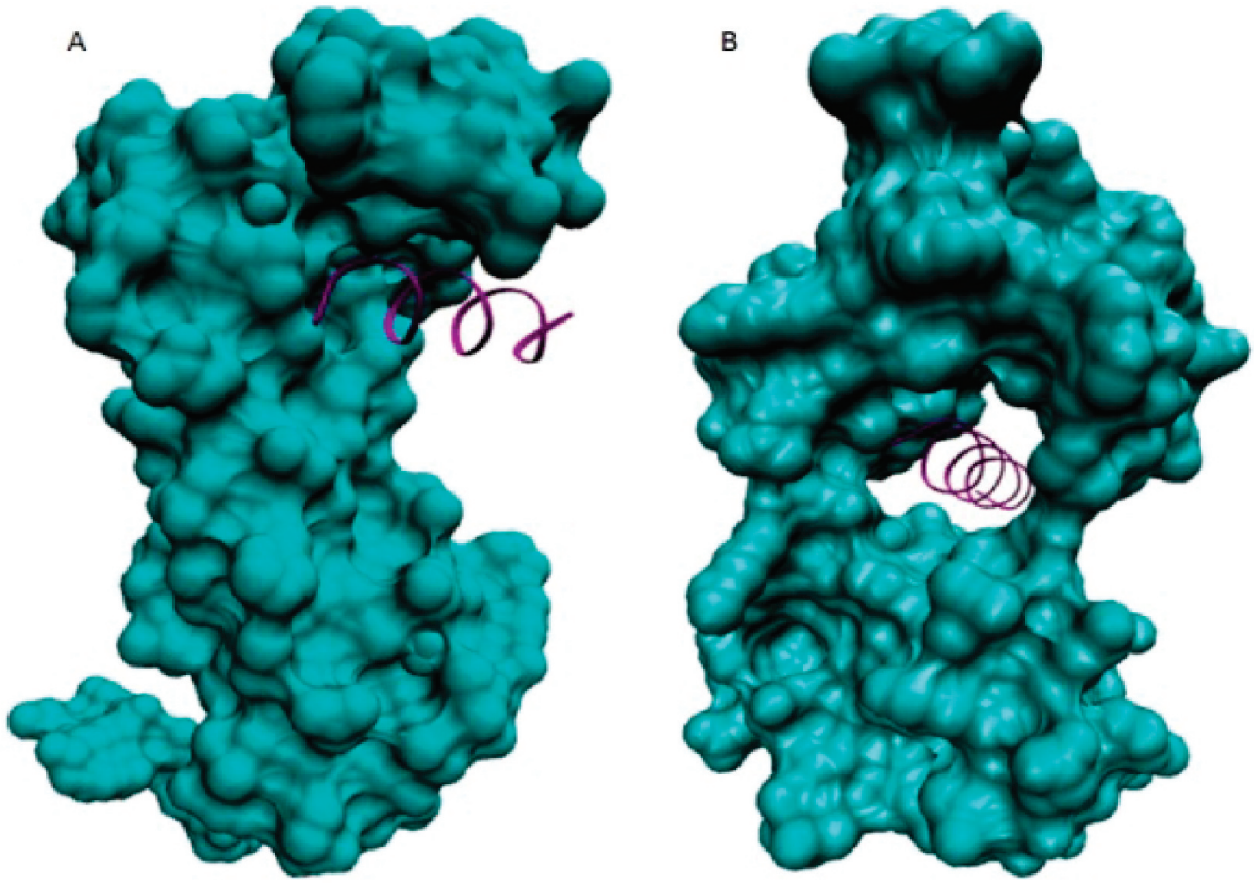

Figure 1. Crystal structures of the MTIP−MyoA complex with MTIP in connoly surface representation and colored cyan and the MyoA in ribbon representation and colored purple. (A) *P. knowlesi* MTIP in complex with the *P. yoelii* MyoA tail, also known as the open form (pdb code: 2AUC). (B) *P. falciparum* MTIP with the MyoA tail, also known as the closed form (pdb code: 2QAC).

to the survival of the parasite is the interaction between myosin motor components in apicomplexan parasites.

Myosins are components of molecular motors present in all eukaryotic cells that are critical for numerous cellular processes, such as organelle transport, mitosis, and cell movement.[15] The apicomplexan myosin, called myosin A (MyoA) in this study, is different from the classical myosin heavy chains and is defined by the lack of a neck or a tail domain; the functional specificity of this myosin is mediated by factors that interact with the myosin light chain.[16] The *P. falciparum* MyoA is a type XIVa myosin, 818 amino acids long, with a head domain consisting of the conserved ATP and actin binding sites.[17] Expression profiling at both the mRNA and protein levels has shown that MyoA is expressed in each of the three invasive forms of *P. falciparum* (sporozoite, merozoite, and ookinete). In the apicomplexan parasites, the actin−MyoA motor complex is a key player in the gliding motility of the parasite that is responsible for the invasion process.[18,19] Initial studies on *P. yoelii* using the yeast two-hybrid system identified the MyoA-associated myosin light chain, which was designated myosin tail interacting protein (MTIP).[18] MTIP is 204 amino acids long, is expressed in all *Plasmodium* invasive life stages, and is colocalized with MyoA. MTIP shows distant sequence homology to the myosin light chains and the calmodulin family of the higher species but lacks the canonical calcium-binding motif.[20]

The crystal structures of the 120 residues of the carboxy terminal and the 140 residues of *P. knowlesi* and *P. falciparum* MTIP, respectively, in complex with the MyoA tail of *P. yoelii* and two structures of *P. knowlesi* MTIP without the bound MyoA tail have been determined (pdb codes 2AUC and 2QAC).[20,21] The carboxy or C-terminal regions of MTIP contain two domains of roughly equal size of which the amino or N-terminal domain is essentially the same in all structures; the C-terminal domain undergoes major conformational change when binding the MyoA-tail α helix. The *P. knowlesi* structure obtained at cryogenic temperatures adopts an "open conformation," with the C-terminal domain providing most of the interactions (Figure 1A). At neutral pH, *P. falciparum* MTIP in complex with the MyoA tail adopts a "closed conformation," with its two domains completely surrounding the MyoA tail helix (Figure 1B). However, in both conformations, the interactions of the MyoA helix with the N-terminal domain of MTIP are limited, and the C-terminal domain of MTIP provides a deep hydrophobic groove to which the MyoA-tail helix binds. Crystal structures of MTIP in complex with MyoA indicate that the MyoA binding site is formed by the residues from the noncalcium-binding EF-hand region of MTIP.

During invasion by malaria parasites, a critical interaction occurs between the MTIP and the MyoA that facilitates the gliding action of the parasite.[18] Previous studies have shown that a 15 amino acid long synthetic MyoA peptide inhibited the growth of *P. falciparum* parasites, whereas the randomized 15-mer or mutant forms of the peptide had no effect on parasite growth.[20] Thus inhibition of this crucial protein−protein interaction by either peptide or small molecules

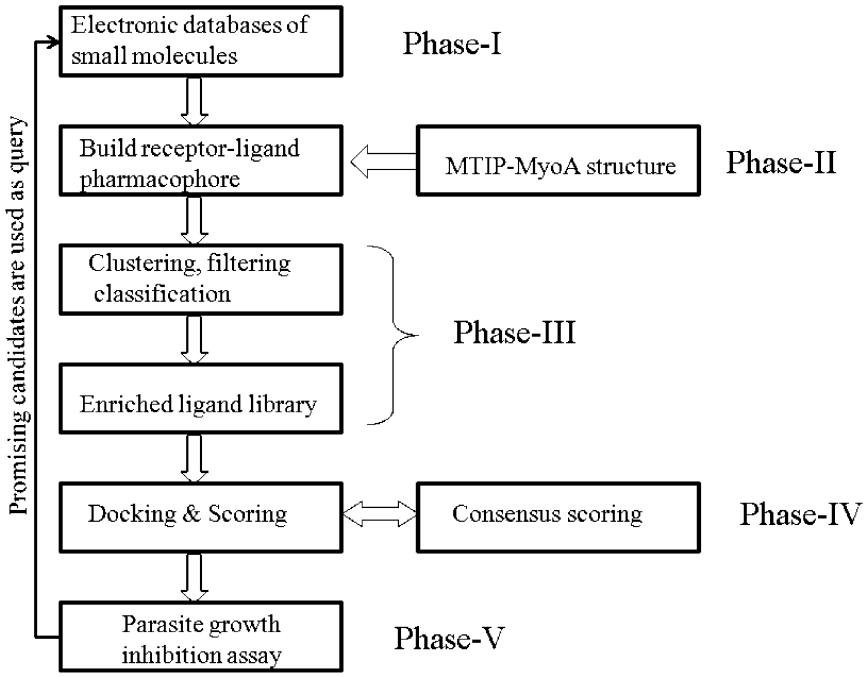

Figure 2. Flowchart of the iterative hybrid structure-based method is shown with the various phases described as follows: phase I: To build a comprehensive electronic database of vendor available small molecules. Phase II: Develop and screen compounds using a hybrid receptor−ligand pharmacophore starting from the three-dimensional structure of the MTIP−MyoA complex. Phase III: Subject compounds that pass the hybrid pharmacophore screening of clustering, filtering, and chemical space analysis to develop the enriched database of small molecules. Phase IV: Dock the molecules selected from the enriched database to the receptor binding site and score them using consensus scoring schemes. Phase V: Test best-ranking compounds for their ability to inhibit parasite growth. The best-ranking compounds from the initial screen will be used as query molecules for iterative screens.

should impede the entry of the parasite into the host cell. We adopted a strategy to design antimalarial compounds that target a MTIP−MyoA interaction found exclusively in *Plasmodium* and other apicomplexan protozoa. This approach not only ensures selectivity of the drug for the parasite over the human host but also drastically reduces the likelihood of parasite resistance because the drug inhibits a key protein−protein interaction that forms the components of the parasite's vulnerable invasive machinery. The drug discovery paradigm used in this study is known as the hybrid structure-based (HSB) method.[22] We customized the HSB method to design inhibitors of protein−protein interaction between MTIP and MyoA using a pharmacophore to screen a library of nearly 300 000 compounds. Several compounds with EC_{50} values less than 1 μM were identified to inhibit parasite growth, and one of them showed significant inhibition of the gliding motility of the parasites.

METHODS

HSB Method for Identifying Potential Lead Molecules. The HSB scheme of virtual screening[22] was used to identify small-molecule compounds that bind to MTIP and that thereby disrupt the requisite MTIP−MyoA interaction. The HSB protocol consists of four major steps (Figure 2): (i) modeling the open form of the *P. falciparum* MTIP−MyoA complex; (ii) designing a pharmacophore model derived from computational analysis of key molecular interactions between MyoA and MTIP in the complex; (iii) screening the small-molecule library with the pharmacophore to identify hits; and (iv) docking hits to MTIP and ranking MTIP−ligand complexes using customized scoring techniques. The top ranking hit compounds were tested for their ability to hinder parasite growth.

Comprehensive Electronic Database of Small Molecules. This database of 300 000 molecules was generated using a subset of the Zinc database[23] that consists of compounds from commercial vendors such as Asinex (Moscow, Russia), Maybridge (Trevillett, North Cornwall, U.K.), Bionet Research (Camelford, Cornwall, U.K.), Cerep (Paris, France), AMRI (Albany, NY), and TimTec (Newark, DE) along with other compounds from natural sources, ligands from the Protein Data Bank (PDB; http://www.pdb.org/pdb/home/contactUs.do), and FDA-approved drugs. All of the commercially available compounds were acquired as sdf formatted files, converted into the Mol2 format, and energy minimized in SYBYL (Tripos, St. Louis, MO). Further, the molecules in the database were filtered for redundancy and renamed according to their corresponding vendor listing.

Structural Model of the *P. falciparum* MTIP−MyoA Complex. Protein sequences of MTIP of *P. falciparum* (Q8I4W8) and *P. knowlesi* (B3LDA6) were retrieved from the SwissProt repository (swiss-prot@expasy.org) for protein sequences.[24] Sequences were aligned using the sequence alignment program CLUSTALW.[25] *P. falciparum* MTIP shares nearly 80% sequence similarity with that of *P. knowlesi* and is completely conserved among residues that interact with MyoA.[20] Similarly, the MyoA tail of *P. falciparum* shares 98% similarity with the corresponding regions of *P. yoelii*, with just a single amino acid change (R814K) in the MTIP interacting region between *P. yoelii* and *P. falciparum*.[20] Based on the high degree of sequence

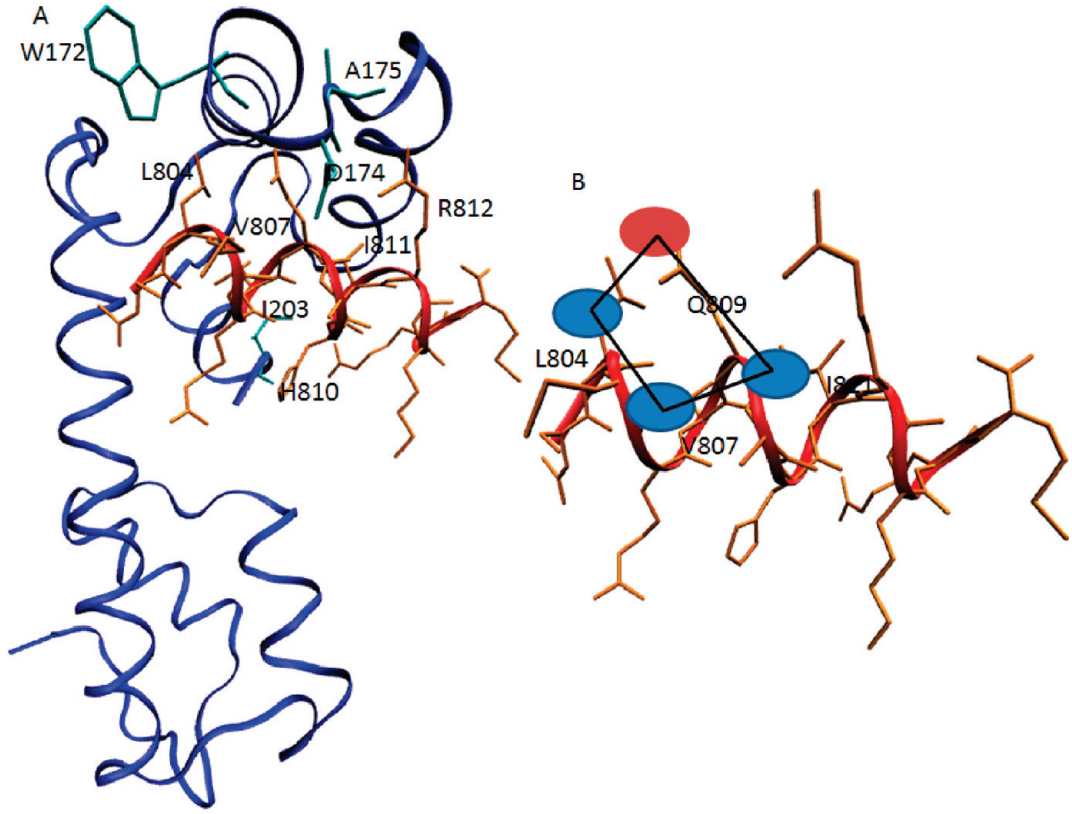

Figure 3. (A) Structural model of the MTIP in complex with MyoA is shown as blue and red ribbons, respectively. Interacting residues from MTIP are depicted as cyan sticks, and the residues of MyoA are rendered as orange sticks. (B) Four-point pharmacophore derived from the interaction of MyoA residues with MTIP is mapped onto the MyoA tail peptide. Blue ovals represent the hydrophobic elements; the red oval represents the hydrophilic elements of the pharmacophore.

homology between *P. knowlesi* and *P. falciparum*, the crystal structure of the MTIP of *P. knowlesi* in complex with the MyoA tail of *P. yoelii* (PDB code: 2AUC) was used as the template to construct an initial structural model of the *P. falciparum* MTIP−MyoA complex. Using the homology modeling program Modeler[26] (version 9.0), three structural models of *P. falciparum* MTIP were built, and the best ranking model was chosen for further docking studies. Similarly, the MyoA tail region of *P. falciparum* was built based on the structure of the MyoA of *P. yoelii*. The modeled MyoA tail was manually docked into the binding site of the MTIP of *P. falciparum*, and the complex was energy minimized using the AMBER force field (version 9).[27]

Virtual Screening Using the Combined Pharmacophore. In the crystal structure, the MyoA tail binds to MTIP with nonbonded interactions. Hydrogen bonds are formed between Gln808, His810, and Arg812 of MyoA and the backbone O and N atoms of Trp172, Asp174, Ala175, and Ile203 of MTIP (Figure 3A). Also, single and cassette mutations of Leu804, Val807, Ile811, and Arg812 of MyoA to alanine resulted in a loss of interaction with MTIP.[20] A four-point structural pharmacophore was built based on these interactions between the MyoA tail and the MTIP in the open form (Figure 3B). The in-house database of small-molecule compounds was screened against the combined pharmacophore using the UNITY module of molecular modeling program SYBYL (version 7.2).[28] To accommodate molecules with different scaffolds and flexible chains, tolerances on the distance constraints of the pharmacophore were set to ±1 Å for hydrophobic elements and to ±2 Å for donor/acceptor elements. Hits that followed the pharmacophore within these tolerances were identified for further computational docking experiments. Because the structure of the pharmacophore was based on the interaction of the MyoA peptide with MTIP and no small-molecule inhibitors of this interaction have been previously identified, the pharmacophore model could not be validated. Instead, a hypothetical small molecule was built by connecting the four pharmacophore atoms (Figure 3B) with the relevant number of carbon chains to fit the pharmacophore and was added to the in-house database.

Docking, Scoring, and Filtering. Virtual screening of the in-house database using the combined pharmacophore yielded 40 hits and the hypothetical small molecule. These 40 small-molecule compounds were then computationally docked to the binding site of MTIP (which was initially occupied by the MyoA tail) using the docking program GOLD (version 3.1).[29] The "library screening mode" option was used for fast docking, and 20 independent docking runs were performed for each ligand to counter the multiple minimum associated with computing the binding energies. Each docked complex was scored using three different scoring functions: goldscore, chemscore, and an in-house customized scoring function.[22] The customized scoring function was designed to identify binding modes of ligands that made essential contacts with binding site residues similar to the ones made by the MyoA tail. These contact scores were then incorporated as a weighting factor to penalize ligand interactions outside the binding site.[22,30] A consensus scoring scheme, based on goldscore, chemscore, and the customized in-house scheme, was used to determine the rankings.[22] The top-ranking molecules were subsequently prioritized with respect to their drug-like properties. The physicochemical properties,

such as logP, molecular weight, and logD, at pH 7.4 were calculated using the program CHEMAXON (version 4.0.5; www.chemaxon.com). The molecules were then filtered by the calculated values of logP and molecular weight. In the initial screening, the Lipinski "rules of 5 criteria"[31] to identify drug-like molecules were strictly used; in subsequent screenings, they were relaxed to accept molecules with molecular weights ≤700 Da (rather than ≤500) and with a computed logP value between 2 and 9 (rather than ≤5). These more relaxed filtering criteria were used to identify molecules that mimicked the large hydrophobic MyoA α helix in the binding site of MTIP. The 15 top-ranking compounds identified from HSB screening were procured and tested in vitro for their ability to hinder the growth of *P. falciparum*. Based on the initial results, compound C416 was used as a query to the iterative HSB method to identify analogs of the compound that shared the pyrazole−urea core with various substitutions to generate the structure−activity relationship (SAR) of the pyrazole−urea series. In these subsequent screenings, the relaxed Lipinski rules were applied to identify all compounds that possessed the pyrazole−urea or amide core to aid SAR studies.

Clustering and Principal Component Analysis. Principal component analysis has been used in a number of studies to analyze the structural diversity among databases or groups of small molecules.[30,32] To assess the uniqueness of our compounds, 6 initial hits from our screening were combined with 63 other antimalarial compounds retrieved from Pubchem (http://pubchem.ncbi.nlm.nih.gov/). Molecular descriptors, such as molecular weight, logP, and MACCS structural keys, were computed using MOE (version 2009.10).[33] Further, the compounds were clustered on the basis of fingerprints computed from MACCS structural keys. To map the chemical and structural class of our hits against the known antimalarial compounds, principal component analysis was done using the cluster codes, molecular weight, and logP values, and the eigenvectors were plotted.

Parasite Growth Inhibition Assays. The best-ranking compounds resulting from in silico HSB screening were tested in the standard *P. falciparum* growth inhibition assays using ^{3}H-hypoxanthine incorporation as a measure of growth over a 48 h period.[34] This assay has been used extensively to screen compounds and has proved to be an excellent parameter for an initial assessment of the efficacy of different compounds.[35] All compounds were purchased from commercial vendors and had a purity of greater than 95%; compound C416-r was synthesized in-house starting from C416. The purity of C416-r was 98% and was assessed using NMR studies. Two starting concentrations, 25 and 12.5 μM, were tested to find compounds with EC_{50} values of <1 μM. Those showing such activity were then tested over a full range of concentrations in triplicate to establish the EC_{50} values for each compound. The assays were performed on the multidrug resistant strain Dd2 of *P. falciparum*.

Parasite Gliding Motility Assays. The ability of compounds with antiparasitic activity to affect sporozoite motility was tested using the rodent malaria parasite *P. berghei*. As sporozoites move, they leave behind trails of shed proteins that can be visualized and quantified. Sporozoites were obtained from salivary glands of infected mosquitoes; the gliding motility assay was performed as described by Coppi et al.[36] Glass eight-chambered Lab-Tek wells (Nalgene; Nalge Nunc, Rochester, NY) were coated with 10 μg/mL of monoclonal antibody 3D11, directed against the repeat region of the circumsporozoite protein, in phosphate-buffered saline (PBS) overnight at 25 °C and then washed three times with PBS prior to the addition of sporozoite. Circumsporozoite protein is one of the most abundant proteins found in the trails, and precoating the wells with antibody more efficiently captured shed circumsporozoite protein onto the slide for visualization. Sporozoites were preincubated with 10 μM of C3-21 or solvent alone in Dulbecco's modified eagle medium with 3% bovine serum albumin (BSA) for 10 min at 28 °C and then added to the coated Lab-Tek wells in the continued presence of the inhibitor in the same medium for 1 h at 37 °C; the medium was removed, and the wells were fixed with 4% paraformaldehyde, washed, and blocked with PBS-1% BSA for 1 h at 37 °C. To visualize the trails, the wells were incubated with biotinylated mAb 3D11 followed by streptavidin−fluorescein isothiocyanate (1:100 dilution; Amersham Pharmacia, GE Healthcare, Piscataway, NJ).

RESULTS AND DISCUSSION

During invasion by malaria parasites, a critical interaction occurs between the MTIP and MyoA that facilitates the gliding action of the parasite.[18] Previous studies have shown that a 15 amino acid long synthetic MyoA peptide inhibited the growth of *P. falciparum* parasites, whereas the randomized 15-mer or mutant forms of the peptide had no effect on parasite growth.[20] Thus, we hypothesized that inhibition of this crucial protein−protein interaction by small molecules that mimic MyoA peptide should impede the entry of the parasite into the host cell.

A three-dimensional structural model of *P. falciparum* MTIP in complex with the MyoA tail peptide in the open form was created using the MTIP-MyoA complex of *P. knowlesi* as a template for the homology modeling program Modeler (version 9.0).[26] Superposition of the backbone atoms of the best-ranking model in relation to that of the crystal structure showed a root-mean-squared deviation of 1.27 Å. Site-directed mutagenesis studies have helped identify key residues on the MyoA helix that interact with MTIP. The MyoA peptide is composed of 13 amino acids that forms an α helix and that fits inside the groove of the MTIP-C subunit (Figure 3A). Leu804, Val807, and Ile811 of the MyoA peptide form the hydrophobic triad and interact with the hydrophobic groove, whereas Gln808 and His810 form hydrogen bonds with MTIP. Other electrostatic interactions include salt bridges between Arg812 and Arg814 of MyoA with Glu180 and Asp202 of MTIP, respectively. Mutagenesis of Leu804, Val807, Ile811, Arg812, and Arg814 residues of MyoA to alanine have resulted in the loss of activity at MTIP.[20] A four-point structural pharmacophore was built on the basis of these interactions involving the hydrophobic triad residues and Gln808 of the MyoA tail with MTIP in the modeled open form (Figure 3B).

The HSB method integrates both ligand- and structure-based methods of virtual screening of chemical databases; hence, it is particularly well suited for the discovery of small-molecule inhibitors of protein−protein interactions (Figure 2). The HSB method was developed as an internal tool to integrate the various ligand- and receptor-based programs

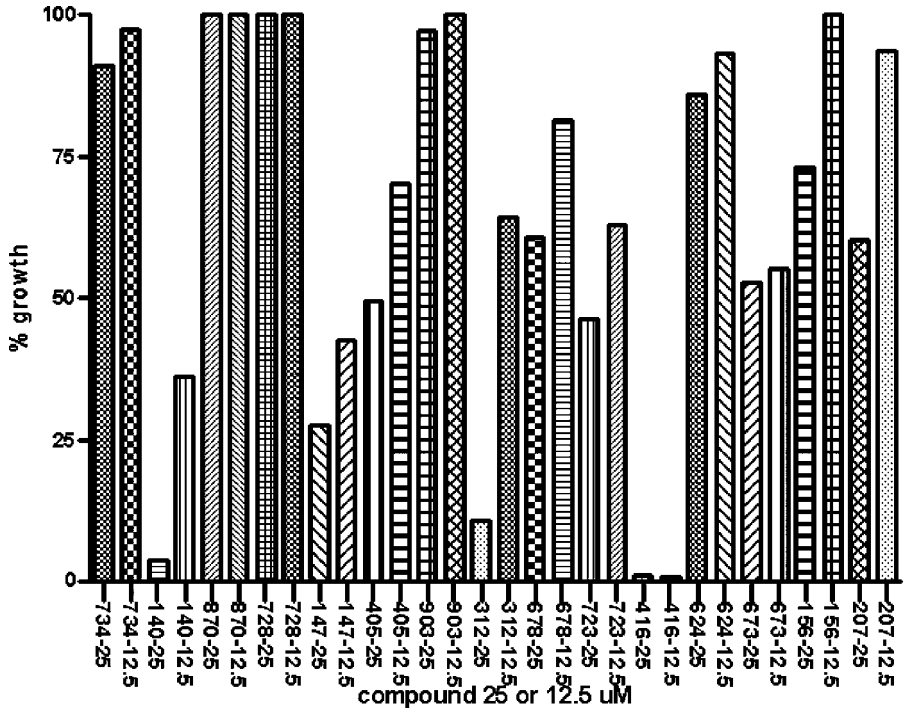

Figure 4. Growth inhibition assay as judged by ^{3}H-hypoxanthine incorporation for the initial 15 compounds tested in concentrations of 25 and 12.5 μM. Compound C416 was used as the lead for further investigation to derive the SAR of pyrazole ureas.

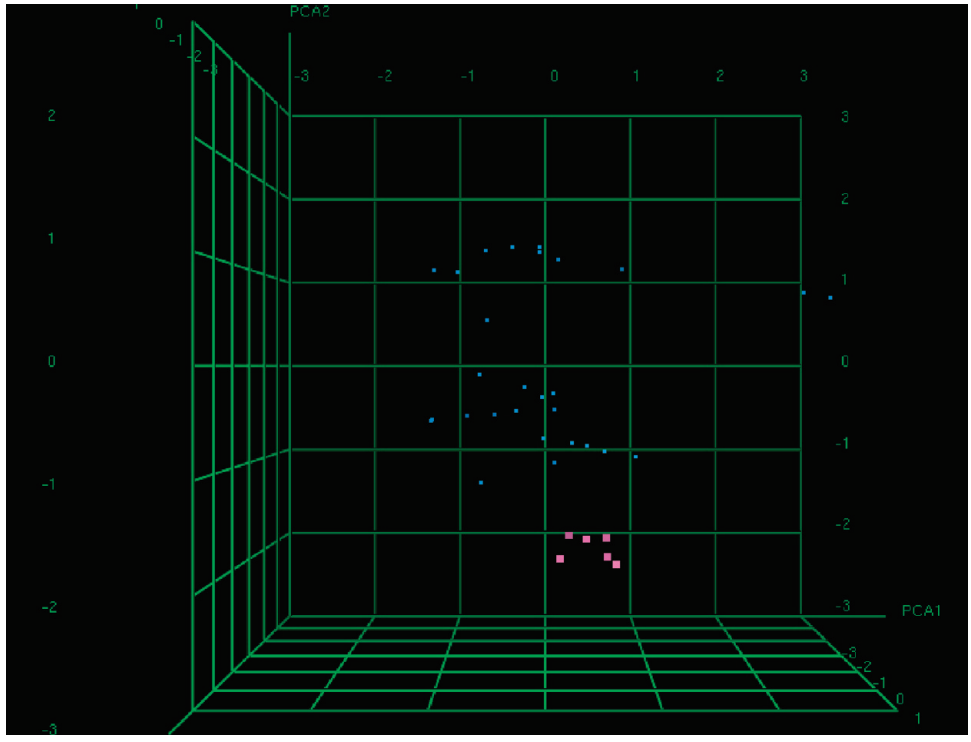

Figure 5. Principal component analysis of antimalarial compounds using cluster codes computed from MACCS structural keys, logP, and molecular weight descriptors. Six antimalarial compounds, shown as pink dots, designed using the HSB method cluster away from the rest of the molecules, representing their unique structural and chemical class.

and to customize them for each specific target.[22] Several published articles that use commercially available docking and scoring functions have shown that no one docking program or scoring function can provide docking solutions that can be used to design inhibitors.[37] To develop a practical application for drug discovery, the essential docking and scoring function should be customized to the target protein. The HSB scheme of virtual screening was used to identify compounds from an in-house database of 300 000 structurally diverse chemicals. Using a four-point pharmacophore (Figure 3B), the small-molecule database was queried to identify 40 compounds that were docked using the GOLD program.[29] The protein−ligand complexes were scored with the customized scoring function described elsewhere.[22,30] The 15 top-ranking hits that passed drug-like property filters were selected for in vitro *P. falciparum* growth inhibition. All 15 compounds were tested at 25 and 12.5 μM; 6 of them exhibited growth inhibitory activity against *P. falciparum*

Table 1. SARs of Pyrazole−urea Compounds Designed Using the Hybrid Structure-Based Method

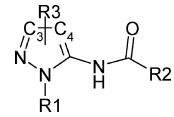

Compound	R1	R2	C3-R3	C4-R3	EC_{50}
C2-1	methyl	1-ethyl-2-fluorobenzene	trifluoromethyl	1-bromo-4-methylbenzene	47nM
C2-2	methyl	methyl	trifluoromethyl	1-bromo-4-methylbenzene	1-10uM
C2-3	methyl	2-methylfuran	trifluoromethyl	1-methoxy-4-methylbenzene	1-10uM
C2-4	methyl	neopentane	trifluoromethyl	1-methoxy-4-methylbenzene	1-10uM
C2-5	methyl	neopentane	trifluoromethyl	1-methyl-3-(trifluoromethyl)benzene	10-100uM
C2-6	methyl	2-methylcyclobutanecarboxylic acid	trifluoromethyl	1-bromo-4-methylbenzene	>100uM
C2-7	methyl	2-(ethylthio)acetic acid	trifluoromethyl	1-methoxy-4-methylbenzene	10-100uM
C2-8	methyl	3-methylpyrazine-2-carboxylic acid	trifluoromethyl	1-bromo-4-methylbenzene	>100uM
C2-9	methyl	3-methylpyrazine-2-carboxylic acid	trifluoromethyl	1-methoxy-4-methylbenzene	>100uM
C2-10	methyl	3-methylpyrazine-2-carboxylic acid	trifluoromethyl	1-methyl-3-(trifluoromethyl)benzene	>100uM
C2-11	methyl	3-methylpyrazine-2-carboxylic acid	trifluoromethyl	1-fluoro-4-methylbenzene	>100uM
C416	methyl	2,4-difluoro-*N*-methylaniline	trifluoromethyl	1-methoxy-4-methylbenzene	145nM
C2-12	methyl	2,4-difluoro-*N*-methylaniline	trifluoromethyl	1-bromo-4-methylbenzene	136nM
C2-13	methyl	2,4-difluoro-*N*-methylaniline	trifluoromethyl	1-fluoro-4-methylbenzene	336nM
C416-r	methyl	2,4-difluoro-*N*-methylaniline	trifluoromethyl	*p*-cresol	3916nM
C2-14	methyl	*N*,2-dimethylpropan-2-amine	trifluoromethyl	1-methoxy-4-methylbenzene	1-10uM
C2-15	methyl	3-methoxy-*N*-methylaniline	trifluoromethyl	1-methyl-3-(trifluoromethyl)benzene	<1uM
C2-16	methyl	toluene	trifluoromethyl	1-methoxy-4-methylbenzene	1-10uM
C2-17	methyl	3-methylpyridine	trifluoromethyl	1-bromo-4-methylbenzene	1-10uM
C2-18	methyl	1,2-dimethoxy-4-methylbenzene	trifluoromethyl	1-methoxy-4-methylbenzene	1-10uM
C2-19	methyl	*N*-methylaniline	trifluoromethyl	1-fluoro-4-methylbenzene	282nM
C2-20	methyl	*N*,4-dimethylbenzenesulfonamide	trifluoromethyl	1-fluoro-4-methylbenzene	10-100uM
C2-21	methyl	4-fluoro-*N*-methylaniline	trifluoromethyl	1-methyl-4-(trifluoromethyl)benzene	342nM
C2-22	methyl	1-fluoro-4-methylbenzene	trifluoromethyl	toluene	1-10uM
C2-23	methyl	3-(*tert*-butyl)-1,5-dimethyl-1*H*-pyrazole	trifluoromethyl	toluene	>100uM
C2-24	methyl	1-methoxy-4-methylbenzene	trifluoromethyl	toluene	10-100uM
C2-25	methyl	2-methylfuran	trifluoromethyl	1-methyl-4-(trifluoromethyl)benzene	10-100uM
C3-1	methyl	4-((benzyloxy)methyl)-*N*-methylaniline	1-chloro-4-methylbenzene	hydrogen	>10uM
C3-2	toluene	4-((benzyloxy)methyl)-*N*-methylaniline	toluene	hydrogen	>10uM
C3-3	methyl	*N*-methylaniline	1-chloro-4-methylbenzene	hydrogen	>10uM
C3-4	methyl	*N*-methyl-4-(trifluoromethyl)aniline	toluene	hydrogen	~10uM
C3-5	methyl	4-(*tert*-butyl)-*N*-methylaniline	toluene	hydrogen	>10uM
C3-6	methyl	*N*,3,5-trimethylaniline	toluene	hydrogen	>10uM
C3-7	methyl	4-fluoro-*N*-methylaniline	toluene	hydrogen	>10uM
C3-8	methyl	*N*-methyl-2,5-dihydrothiophen-3-amine	toluene	hydrogen	>10uM
C3-9	methyl	2-fluoro-*N*-methylaniline	toluene	hydrogen	>10uM
C3-10	methyl	*N*,2-dimethylaniline	toluene	hydrogen	>10uM
C3-11	methyl	4-chloro-*N*-methylaniline	toluene	hydrogen	>10uM
C3-12	toluene	4-chloro-*N*-methylaniline	methylcyclopropane	hydrogen	>10uM
C3-13	hydrogen	3,5-dichloro-*N*-methylaniline	toluene	hydrogen	>10uM
C3-14	hydrogen	3,5-dichloro-*N*-methylaniline	2-methylthiophene	hydrogen	>10uM
C3-15	hydrogen	3,5-dichloro-*N*-methylaniline	2-methylfuran	hydrogen	>10uM
C3-16	hydrogen	*N*-methyl-4-(trifluoromethoxy)aniline	toluene	hydrogen	>10uM
C3-17	hydrogen	*N*-methylaniline	toluene	hydrogen	>10uM
C3-18	1,2-dichloro-4-methylbenzene	2-(methylamino)benzonitrile	1-methoxy-4-methylbenzene	hydrogen	~10uM
C3-19	1-fluoro-4-methylbenzene	4-(benzyloxy)-*N*-methylaniline	2-methylthiophene	hydrogen	>10uM
C3-20	1,2,4-trimethylbenzene	*N*-methyl-4-(trifluoromethoxy)aniline	1-methyl-4-(trifluoromethoxy)benzene	hydrogen	300nM
C3-21	1-fluoro-4-methylbenzene	*N*-methyl-4-(trifluoromethoxy)aniline	1-chloro-4-methylbenzene	hydrogen	385nM
C3-22	toluene	hydrogen	2-methylthiophene	(*E*)-4-ethylidene-5-methylene-2-phenyl-4,5-dihydrooxazole	>10uM
C3-23	1,2,4-trimethylbenzene	2-(methylamino)benzonitrile	1-methyl-4-(trifluoromethoxy)benzene	hydrogen	5.3uM
C3-24	toluene	hydrogen	2-methylthiophene	(*E*)-*N'*-ethylidenethiophene-2-carbohydrazide	4uM
C3-25	toluene	hydrogen	toluene	1-(2,4-difluorophenyl)-3-methylurea	13.2uM

* C3-22, C3-24, and C3-25 do not have the same connectivity as the parent compound; the urea group with R2 is replaced by H in all three cases.

exceeding 50% at 25 μM (Figure 4). Further, a clustering of all six compounds based on their MACCS structural keys and other physicochemical properties, along with other antimalarial compounds chosen from the PubChem database,[38] suggested that these six compounds belonged to unique chemical classes, and hence, each might represent novel antimalarial lead compounds (Figure 5). Analysis of their docking mode in the MTIP binding site revealed that all six compounds occupied the same binding site as that of the MyoA peptide in the crystal structure. The compounds in their docked conformation interacted with Leu169, Ile203, Phe199, Ala184, Leu176, Leu145, and Phe149 and also with Asp174 and Trp172 in the binding site of MTIP. However, no hydrogen-bonding interactions with MTIP residues were observed for any of the six inhibitor molecules. This observation led us to speculate that MTIP may or may not be the intended target of these compounds and that the compounds may bind to other proteins in addition to MTIP with similar binding pockets. Among the six compounds, C416 was the most potent inhibitor (EC_{50} = 145 nM); it was, therefore, chosen as the lead compound to derive analogs using the iterative HSB method.

SAR of Pyrazole−Urea Compounds. Using the pyrazole−urea compound C416 as the query, 51 analogs were identified to develop the SAR of this class of compounds (Table 1). Docking studies predicted that all of these molecules bind to MTIP at the same site as the parent compound C416. Structural analysis of the proposed docking mode of the pyrazole−urea compounds in the MTIP binding site suggested that the R1 group has interactions with Phe149, Met148, and Leu145, that R2 interacts with Gly173, Leu176, and Ala175, and that R3 interacts with Asn167, Ile168, Leu169, and Thr171. The urea core interacts with Trp172 and Asp174 within a distance of 4.5−5 Å (Figure 6). The pharmacophore elements fit to the three hydrophobic rings and the amine of the urea core (Figure 6B). On the basis of the docking mode of C416 in MTIP, positions R2 and R3 were modified conservatively to retain their hydrophobicity and aromatic features. The methyl group at position R1 in C416 was systematically replaced by a proton and/or by

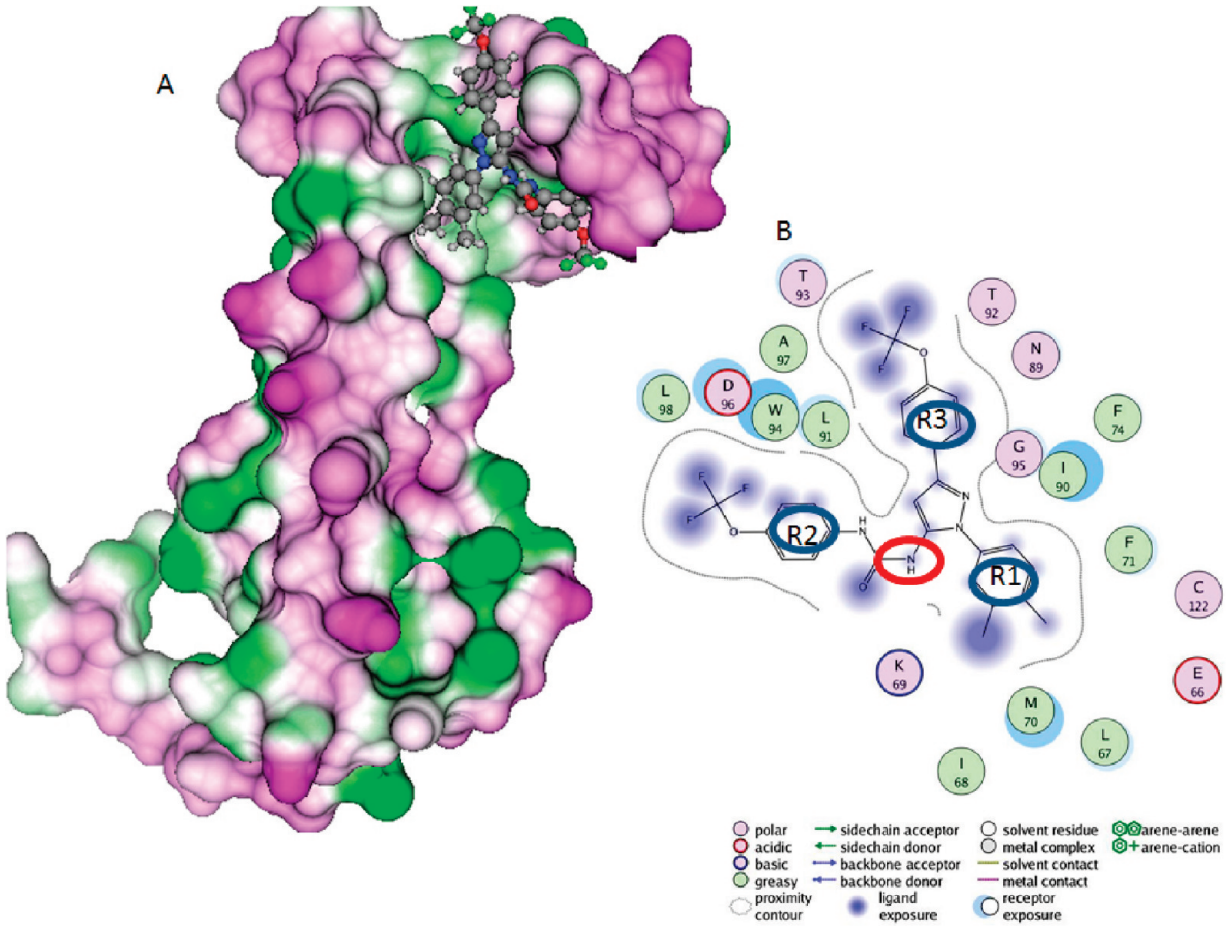

Figure 6. Structural model of MTIP in complex with C3-20 is shown. (A) MTIP is shown in a Connolly surface representation and is colored based on its hydrophobicity (scale: hydrophilic, pink; neutral, white; hydrophobic, green). C3-20 is represented in ball and stick model; the atoms are colored as follows: carbon, gray; nitrogen, blue; oxygen, red; fluorine, green; hydrogen, white. (B) Schematic representation of C3-20 in the binding site of MTIP using program MOE (version 2009.10), with SAR components R1, R2, and R3 (see Table 1 for examples) labeled and mapped with the pharmacophore elements (hydrophobic in open blue ovals and donor/acceptor pair in open red oval).

aromatic groups. R3 was replaced with either a hydrogen atom or an aromatic group at either the C3 or C4 carbon atom of the pyrazole ring. Changing the urea core to an acetamide did not affect the activity of the compounds; however, an increase or decrease in the length of the linker group between the pyrazole and R2 rings drastically reduced the activity irrespective of the other substitutions. Compound C2-1 had the best inhibitory profile against the parasite growth with an EC_{50} value of 47 nM. C2-1 was similar to C416 with a pyrazole−acetamide core instead of a pyrazole−urea core. Among the 52 pyrazole compounds that were tested that included the parent C416, eight compounds had EC_{50} values <400 nM. Among these active compounds, C2-1, C21-12, C416, C2-19, C2-13, and C2-21 shared similar structural elements, and their EC_{50} values ranged from 45 to 342 nM. The SAR of compounds C416, C2-12, C2-13, and C416-r showed that changing the hydrophobic bromine group at the para position on the R3 ring attached to the C4 carbon of the pyrazole ring (in C2-12) to the more hydrophilic hydroxyl group (in C416-r) reduced the affinity by about 30-fold. This position preferred a more hydrophobic group with an activity pattern −Br > OMe > F > OH. Similarly, at position R2, removing fluorine atoms from the ortho and para positions led to a minor improvement in the EC_{50} values from 336 (C2-13) to 282 nM for C2-19. In other compounds, such as C3-18, C3-19, C3-20, C3-21, and C3-23, the methyl group at R1 was substituted with an aromatic group, and the aromatic R3 group was bonded to the C4 atom of the pyrazole ring instead of to the C3 atom. These compounds were moderately active, with EC_{50} values ranging from 300 nM to 10 μM. Major modification to the structure by shifting the urea linker to the C4 carbon on the pyrazole ring yielded 3-25, a compound with an EC_{50} value of about 13 μM. Apart from these highly active compounds, the screening also led to the identification of 10 new compounds with EC_{50} values between 1 and 10 μM (C2-2, C2-3, C2-4, C2-15, C2-16, C2-17, C2-18, C2-22, C3-4, and C3-24).

Plasmodium sporozoites and other apicomplexans exhibit a unique substrate-dependent locomotion called gliding motility that is critical for the cellular invasion process.[18] Since our compounds were hypothesized to inhibit MTIP, they must also inhibit the gliding motility of the parasites. Compounds C2-1 and C3-21 that represented the two subclasses (with swapped substitutions at R1 and C4 atom) were tested for their ability to interfere with gliding motility in the invasion assays. The untreated sporozoites showed a typical circular gliding motility observed by immunofluorescence staining of the circumsporozoite protein trail, whereas the movement of sporozoites treated with compound C3-21 was impaired (Figure 7), providing indirect evidence that some of the pyrazole−urea compounds inhibited MTIP−MyoA interaction.

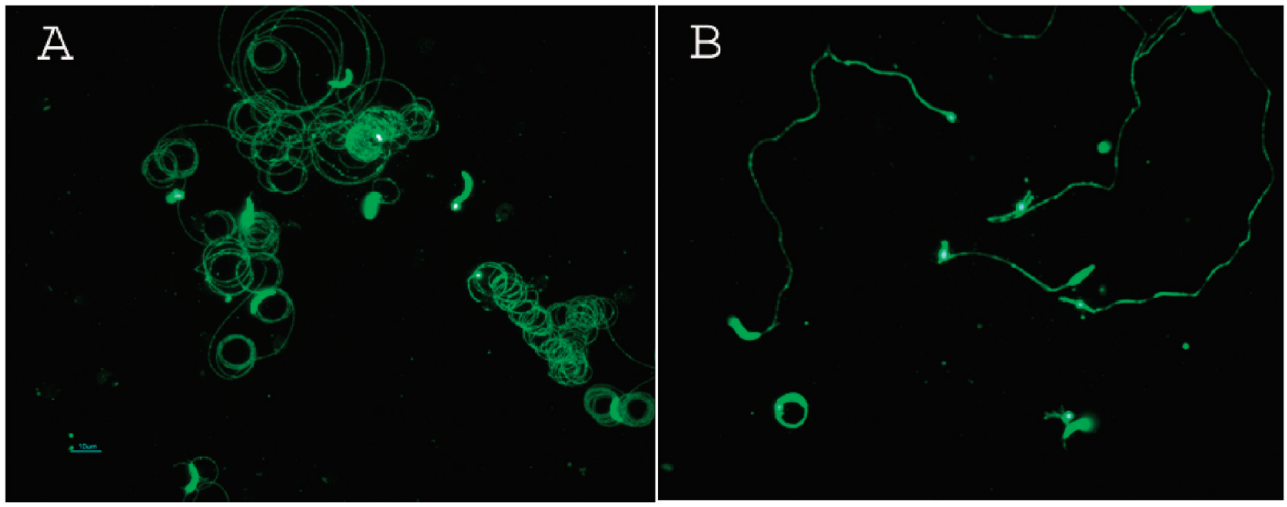

Figure 7. Inhibition of *P. berghei* sporozoite gliding motility by the pyrazole−urea compound C3-21. (A) Solvent-treated sporozoites show typical circular gliding motility observed by indirect fluorescent antibody staining of the circumsporozoite protein trail. (B) The compound C3-21 treated sporozoites are highly impaired in their movement.

CONCLUSIONS

During invasion by malarial parasites, a critical interaction occurs between the myosin motor components myosin A (MyoA) and myosin tail interacting protein (MTIP). Most of the MTIP residues engaged in critical interactions with MyoA are conserved among all of the *Plasmodium* species. Thus, MTIP−MyoA inhibitors should effectively block all of the invasive stages. Small-molecule compounds that block the MTIP−MyoA interaction complex offer promise as antimalarial compounds because they block the invasion process. The compounds were designed to inhibit a specific protein−protein interaction, thereby greatly diminishing the likelihood of acquired drug resistance by the parasite through permissible complementary mutations of interacting residues on both MTIP and MyoA. Using the hybrid structure-based (HSB) method, we successfully designed eight compounds (C416, C2-1, C2-12, C2-13, C2-19, C2-21, C3-20, and C3-21) belonging to the unique pyrazole−urea class that inhibit the growth of the malarial parasite and alter the gliding motility of rodent malaria sporozoites. Although the compounds possess a novel structural core, they are very hydrophobic (ClogP values >5) and are soluble only in dimethyl sulfoxide (DMSO). The limited solubility of these compounds in other solvents has hampered the ability to use other biophysical experiments, such as surface plasmon resonance, thermal melt, and crystallization studies, to provide direct evidence for the mechanism of action of these compounds. Studies to improve the solubility of the compounds and to provide direct evidence of their binding to MTIP are ongoing.

ACKNOWLEDGMENT

We would like to thank Dr. Eric Wang for the synthesis of compound C416-r. P.S. was supported by a National Institutes of Health (NIH) grant R01 AI056840. I.E. was supported by a Research Supplement to Promote Diversity in Health-Related Research to R01 AI056840 and a Medical Scientist Training Program grant T32 GM07308. W.J.W. acknowledges support provided for this work by the US Environmental Protection Agency-funded Environmental Bioinformatics and Computational Toxicology Center (STAR grant GAD R 832721-010), the Defense Threat Reduction Agency (HDTRA-BB07TAS020), and the NIH-National Institute of General Medical Sciences (R21-GM081394). L.W.B. acknowledges support provided by the NIH (R01 AI068137). A.B.V. acknowledges support provided by a grant from the Pennsylvania Commonwealth Universal Research Enhancement (CURE) Program. This work has not been reviewed by and does not represent the opinions of the funding agencies.

REFERENCES AND NOTES

(1) Snow, R. W.; Guerra, C. A.; Noor, A. M.; Myint, H. Y.; Hay, S. I. The global distribution of clinical episodes of Plasmodium falciparum malaria. *Nature* **2005**, *434*, 214–217.

(2) (a) Sachs, J.; Malaney, P. The economic and social burden of malaria. *Nature* **2002**, *415*, 680–685. (b) Malaney, P.; Spielman, A.; Sachs, J. The malaria gap. *Am. J. Trop. Med. Hyg.* **2004**, *71* (2), 141–146.

(3) Sengaloundeth, S.; Green, M. D.; Fernandez, F. M.; Manolin, O.; Phommavong, K.; Insixiengmay, V.; Hampton, C. Y.; Nyadong, L.; Mildenhall, D. C.; Hostetler, D.; Khounsaknalath, L.; Vongsack, L.; Phompida, S.; Vanisaveth, V.; Syhakhang, L.; Newton, P. N. A stratified random survey of the proportion of poor quality oral artesunate sold at medicine outlets in the Lao PDR - implications for therapeutic failure and drug resistance. *Malar. J.* **2009**, *8*, 172.

(4) AlKadi, H. O. Antimalarial drug toxicity: a review. *Chemotherapy* **2007**, *53*, 385–391.

(5) (a) Gero, A. M.; O'Sullivan, W. J. Purines and pyrimidines in malarial parasites. *Blood Cells* **1990**, *16*, 467–484, discussion 485−498. (b) Jones, M. E. Pyrimidine nucleotide biosynthesis in animals: genes, enzymes, and regulation of UMP biosynthesis. *Annu. Rev. Biochem.* **1980**, *49*, 253–279.

(6) Phillips, M. A.; Gujjar, R.; Malmquist, N. A.; White, J.; El Mazouni, F.; Baldwin, J.; Rathod, P. K. Triazolopyrimidine-based dihydroorotate dehydrogenase inhibitors with potent and selective activity against the malaria parasite Plasmodium falciparum. *J. Med. Chem.* **2008**, *51*, 3649–3653.

(7) Langley, D. B.; Shojaei, M.; Chan, C.; Lok, H. C.; Mackay, J. P.; Traut, T. W.; Guss, J. M.; Christopherson, R. I. Structure and inhibition of orotidine 5′-monophosphate decarboxylase from Plasmodium falciparum. *Biochemistry* **2008**, *47*, 3842–3854.

(8) Kreidenweiss, A.; Kremsner, P. G.; Mordmuller, B. Comprehensive study of proteasome inhibitors against Plasmodium falciparum laboratory strains and field isolates from Gabon. *Malar. J.* **2008**, *7*, 187.

(9) (a) Biagini, G. A.; Fisher, N.; Berry, N.; Stocks, P. A.; Meunier, B.; Williams, D. P.; Bonar-Law, R.; Bray, P. G.; Owen, A.; O'Neill, P. M.; Ward, S. A. Acridinediones: selective and potent inhibitors of the malaria parasite mitochondrial bc1 complex. *Mol. Pharmacol.* **2008**, *73*, 1347–1355. (b) Kessl, J. J.; Meshnick, S. R.; Trumpower, B. L. Modeling the molecular basis of atovaquone resistance in parasites

and pathogenic fungi. *Trends Parasitol.* **2007**, *23*, 494–501. (c) Winter, R. W.; Kelly, J. X.; Smilkstein, M. J.; Dodean, R.; Hinrichs, D.; Riscoe, M. K. Antimalarial quinolones: synthesis, potency, and mechanistic studies. *Exp. Parasitol.* **2008**, *118*, 487–497. (d) Yeates, C. L.; Batchelor, J. F.; Capon, E. C.; Cheesman, N. J.; Fry, M.; Hudson, A. T.; Pudney, M.; Trimming, H.; Woolven, J.; Bueno, J. M.; Chicharro, J.; Fernandez, E.; Fiandor, J. M.; Gargallo-Viola, D.; Gomez de las Heras, F.; Herreros, E.; Leon, M. L. Synthesis and structure-activity relationships of 4-pyridones as potential antimalarials. *J. Med. Chem.* **2008**, *51*, 2845–2852.

(10) Fan, Q.; Miao, J.; Cui, L. Characterization of PRMT1 from Plasmodium falciparum. *Biochem. J.* **2009**, *421*, 107–118.

(11) Krungkrai, J.; Krungkrai, S. R.; Supuran, C. T. Carbonic anhydrase inhibitors: Inhibition of Plasmodium falciparum carbonic anhydrase with aromatic/heterocyclic sulfonamides-in vitro and in vivo studies. *Bioorg. Med. Chem. Lett.* **2008**, *18*, 5466–5471.

(12) (a) Lemercier, G.; Fernandez-Montalvan, A.; Shaw, J. P.; Kugelstadt, D.; Bomke, J.; Domostoj, M.; Schwarz, M. K.; Scheer, A.; Kappes, B.; Leroy, D. Identification and characterization of novel small molecules as potent inhibitors of the plasmodial calcium-dependent protein kinase 1. *Biochemistry* **2009**, *48*, 6379–6389. (b) Waters, N. C.; Geyer, J. A. Cyclin-dependent protein kinases as therapeutic drug targets for antimalarial drug development. *Expert Opin. Ther. Targets* **2003**, *7*, 7–17.

(13) (a) Li, H.; Huang, J.; Chen, L.; Liu, X.; Chen, T.; Zhu, J.; Lu, W.; Shen, X.; Li, J.; Hilgenfeld, R.; Jiang, H. Identification of novel falcipain-2 inhibitors as potential antimalarial agents through structure-based virtual screening. *J. Med. Chem.* **2009**, *52*, 4936–4940. (b) Linares, G. E.; Rodriguez, J. B. Current status and progresses made in malaria chemotherapy. *Curr. Med. Chem.* **2007**, *14*, 289–314.

(14) (a) Barazarte, A.; Camacho, J.; Dominguez, J.; Lobo, G.; Gamboa, N.; Rodrigues, J.; Capparelli, M. V.; Alvarez-Larena, A.; Andujar, S.; Enriz, D.; Charris, J. Synthesis, antimalarial activity, structure-activity relationship analysis of thieno-[3,2-b]benzothiazine S, S-dioxide analogs. *Bioorg. Med. Chem.* **2008**, *16*, 3661–3674. (b) Carraz, M.; Jossang, A.; Rasoanaivo, P.; Mazier, D.; Frappier, F. Isolation and antimalarial activity of new morphinan alkaloids on Plasmodium yoelii liver stage. *Bioorg. Med. Chem.* **2008**, *16*, 6186–6192. (c) Gupta, L.; Srivastava, K.; Singh, S.; Puri, S. K.; Chauhan, P. M. Synthesis of 2-[3-(7-Chloro-quinolin-4-ylamino)-alkyl]-1-(substituted phenyl)-2,3,4,9-tetrahydro-1H-beta-carbolines as a new class of antimalarial agents. *Bioorg. Med. Chem. Lett.* **2008**, *18*, 3306–3309. (d) Harpstrite, S. E.; Collins, S. D.; Oksman, A.; Goldberg, D. E.; Sharma, V. Synthesis, characterization, and antimalarial activity of novel schiff-base-phenol and naphthalene-amine ligands. *Med. Chem.* **2008**, *4*, 392–395. (e) Henry, M.; Alibert, S.; Baragatti, M.; Mosnier, J.; Baret, E.; Amalvict, R.; Legrand, E.; Fusai, T.; Barbe, J.; Rogier, C.; Pages, J. M.; Pradines, B. Dihydroethanoanthracene derivatives reverse in vitro quinoline resistance in Plasmodium falciparum malaria. *Med. Chem.* **2008**, *4*, 426–437. (f) Kgokong, J. L.; Matsabisa, G. M.; Smithand, P. P.; Breytenbach, J. C. N. N-Bis(trifluoromethylquinolin-4-yl)diamino alkanes: synthesis and antimalarial activity. *Med. Chem.* **2008**, *4*, 438–445. (g) Paunescu, E.; Susplugas, S.; Boll, E.; Varga, R. A.; Mouray, E.; Grellier, P.; Melnyk, P. Synthesis and antimalarial activity of new amino analogues of amodiaquine. *Med. Chem.* **2008**, *4*, 407–425. (h) Sparatore, A.; Basilico, N.; Casagrande, M.; Parapini, S.; Taramelli, D.; Brun, R.; Wittlin, S.; Sparatore, F. Antimalarial activity of novel pyrrolizidinyl derivatives of 4-aminoquinoline. *Bioorg. Med. Chem. Lett.* **2008**, *18*, 3737–3740. (i) Yoshikawa, M.; Motoshima, K.; Fujimoto, K.; Tai, A.; Kakuta, H.; Sasaki, K. Pyridinium cationic-dimer antimalarials, unlike chloroquine, act selectively between the schizont stage and the ring stage of Plasmodium falciparum. *Bioorg. Med. Chem.* **2008**, *16*, 6027–6033.

(15) O'Connell, C. B.; Tyska, M. J.; Mooseker, M. S. Myosin at work: motor adaptations for a variety of cellular functions. *Biochim. Biophys. Acta* **2007**, *1773*, 615–630.

(16) (a) Foth, B. J.; Goedecke, M. C.; Soldati, D. New insights into myosin evolution and classification. *Proc. Natl. Acad. Sci. U.S.A.* **2006**, *103*, 3681–3686. (b) Keeley, A.; Soldati, D. The glideosome: a molecular machine powering motility and host-cell invasion by Apicomplexa. *Trends Cell Biol.* **2004**, *14*, 528–532.

(17) (a) Pinder, J. C.; Fowler, R. E.; Dluzewski, A. R.; Bannister, L. H.; Lavin, F. M.; Mitchell, G. H.; Wilson, R. J.; Gratzer, W. B. Actomyosin motor in the merozoite of the malaria parasite, Plasmodium falciparum: implications for red cell invasion. *J. Cell Sci.* **1998**, *111* (13), 1831–1839. (b) Matuschewski, K.; Mota, M. M.; Pinder, J. C.; Nussenzweig, V.; Kappe, S. H. Identification of the class XIV myosins Pb-MyoA and Py-MyoA and expression in Plasmodium sporozoites. *Mol. Biochem. Parasitol.* **2001**, *112*, 157–161.

(18) Bergman, L. W.; Kaiser, K.; Fujioka, H.; Coppens, I.; Daly, T. M.; Fox, S.; Matuschewski, K.; Nussenzweig, V.; Kappe, S. H. Myosin A tail domain interacting protein (MTIP) localizes to the inner membrane complex of Plasmodium sporozoites. *J. Cell Sci.* **2003**, *116* (Pt 1), 39–49.

(19) (a) Green, J. L.; Martin, S. R.; Fielden, J.; Ksagoni, A.; Grainger, M.; Yim Lim, B. Y.; Molloy, J. E.; Holder, A. A. The MTIP-myosin A complex in blood stage malaria parasites. *J. Mol. Biol.* **2006**, *355*, 933–941. (b) Jones, M. L.; Kitson, E. L.; Rayner, J. C. Plasmodium falciparum erythrocyte invasion: a conserved myosin associated complex. *Mol. Biochem. Parasitol.* **2006**, *147*, 74–84.

(20) Bosch, J.; Turley, S.; Daly, T. M.; Bogh, S. M.; Villasmil, M. L.; Roach, C.; Zhou, N.; Morrisey, J. M.; Vaidya, A. B.; Bergman, L. W.; Hol, W. G. Structure of the MTIP-MyoA complex, a key component of the malaria parasite invasion motor. *Proc. Natl. Acad. Sci. U.S.A.* **2006**, *103*, 4852–4857.

(21) Bosch, J.; Turley, S.; Roach, C.; Daly, T. M.; Bergman, L. W.; Hol, W. G. The closed MTIP-MyosinA-tail complex from the malaria parasite invasion machinery. *J. Mol. Biol.* **2007**, *372*, 77–88.

(22) Kortagere, S.; Welsh, W. J. Development and application of hybrid structure based method for efficient screening of ligands binding to G-protein coupled receptors. *J. Comput.-Aided Mol. Des.* **2006**, *20*, 789–802.

(23) Irwin, J. J.; Shoichet, B. K. ZINC--a free database of commercially available compounds for virtual screening. *J. Chem. Inf. Model.* **2005**, *45*, 177–182.

(24) Bairoch, A.; Apweiler, R. The SWISS-PROT protein sequence database: its relevance to human molecular medical research. *J. Mol. Med.* **1997**, *75*, 312–316.

(25) Thompson, J. D.; Higgins, D. G.; Gibson, T. J. CLUSTAL W: improving the sensitivity of progressive multiple sequence alignment through sequence weighting, position-specific gap penalties and weight matrix choice. *Nucleic Acids Res.* **1994**, *22*, 4673–4680.

(26) Sanchez, R.; Sali, A. Evaluation of comparative protein structure modeling by MODELLER-3. *Proteins* **1997**, (1), 50–58.

(27) Wang, J.; Wang, W.; Kollman, P. A.; Case, D. A. Automatic atom type and bond type perception in molecular mechanical calculations. *J. Mol. Graphics Modell.* **2006**, *25*, 247–260.

(28) Weiner, S. J.; Kollman, P. A.; Nguyen, D. T.; Case, D. A. An all atom force field for simulations of proteins and nucleic acids. *J. Comput. Chem.* **1986**, *7*, 230–252.

(29) Jones, G.; Willett, P.; Glen, R. C.; Leach, A. R.; Taylor, R. Development and validation of a genetic algorithm for flexible docking. *J. Mol. Biol.* **1997**, *267*, 727–748.

(30) Kortagere, S.; Chekmarev, D.; Welsh, W. J.; Ekins, S. Hybrid scoring and classification approaches to predict human pregnane x receptor activators. *Pharm. Res.* **2009**, *26*, 1001–1011.

(31) Lipinski, C. A.; Lombardo, F.; Dominy, B. W.; Feeney, P. J. Experimental and computational approaches to estimate solubility and permeability in drug discovery and development settings. *Adv. Drug Delivery Rev.* **2001**, *46*, 3–26.

(32) Haggarty, S. J.; Clemons, P. A.; Wong, J. C.; Schreiber, S. L. Mapping chemical space using molecular descriptors and chemical genetics: deacetylase inhibitors. *Comb. Chem. High Throughput Screening* **2004**, *7*, 669–676.

(33) *MOE (Molecular Operating Environment)*, version 2009. 10; Chemical Computing Group: Montreal, Quebec, Canada, 2009.

(34) Desjardins, R. E.; Canfield, C. J.; Haynes, J. D.; Chulay, J. D. Quantitative assessment of antimalarial activity in vitro by a semiautomated microdilution technique. *Antimicrob. Agents Chemother.* **1979**, *16*, 710–718.

(35) Painter, H. J.; Morrisey, J. M.; Mather, M. W.; Vaidya, A. B. Specific role of mitochondrial electron transport in blood-stage Plasmodium falciparum. *Nature* **2007**, *446*, 88–91.

(36) Coppi, A.; Cabinian, M.; Mirelman, D.; Sinnis, P. Antimalarial activity of allicin, a biologically active compound from garlic cloves. *Antimicrob. Agents Chemother.* **2006**, *50*, 1731–1737.

(37) (a) Warren, G. L.; Andrews, C. W.; Capelli, A. M.; Clarke, B.; LaLonde, J.; Lambert, M. H.; Lindvall, M.; Nevins, N.; Semus, S. F.; Senger, S.; Tedesco, G.; Wall, I. D.; Woolven, J. M.; Peishoff, C. E.; Head, M. S. A critical assessment of docking programs and scoring functions. *J. Med. Chem.* **2006**, *49*, 5912–5931. (b) Ferrara, P.; Gohlke, H.; Price, D. J.; Klebe, G.; Brooks, C. L. 3rd, Assessing scoring functions for protein-ligand interactions. *J. Med. Chem.* **2004**, *47*, 3032–3047.

(38) Sayers, E. W.; Barrett, T.; Benson, D. A.; Bolton, E.; Bryant, S. H.; Canese, K.; Chetvernin, V.; Church, D. M.; Dicuccio, M.; Federhen, S.; Feolo, M.; Geer, L. Y.; Helmberg, W.; Kapustin, Y.; Landsman, D.; Lipman, D. J.; Lu, Z.; Madden, T. L.; Madej, T.; Maglott, D. R.; Marchler-Bauer, A.; Miller, V.; Mizrachi, I.; Ostell, J.; Panchenko, A.; Pruitt, K. D.; Schuler, G. D.; Sequeira, E.; Sherry, S. T.; Shumway, M.; Sirotkin, K.; Slotta, D.; Souvorov, A.; Starchenko, G.; Tatusova, T. A.; Wagner, L.; Wang, Y.; John Wilbur, W.; Yaschenko, E.; Ye, J. Database resources of the National Center for Biotechnology Information. *Nucleic Acids Res.* **2009**, *37*, D5–D15.

CI100039K